

Dynamic formation of supersolid phase in a mixture of ultracold bosonic and fermionic atoms

Maciej Lewkowicz,¹ Tomasz Karpiuk,² Mariusz Gajda,³ and Mirosław Brewczyk²

¹ *Doctoral School of Exact and Natural Sciences, University of Białystok, ul. K. Ciołkowskiego 1K, 15-245 Białystok, Poland*

² *Wydział Fizyki, Uniwersytet w Białymstoku, ul. K. Ciołkowskiego 1L, 15-245 Białystok, Poland*

³ *Institute of Physics, Polish Academy of Sciences, Aleja Lotników 32/46, PL-02668 Warsaw, Poland*

We numerically study the dynamical properties of a mixture consisting of a dipolar condensate and a degenerate Fermi gas in a quasi-one-dimensional geometry. In particular, we focus on the system's response to a temporal variation in the interaction strength between bosons and fermions. When the interspecies attraction becomes sufficiently strong, we observe a phase transition to a supersolid state. This conclusion is supported by the emergence of an out-of-phase Goldstone mode in the excitation spectrum.

I. INTRODUCTION

Ultracold quantum gases provide a highly controllable platform for exploring complex many-body phenomena in quantum systems. Among the most notable recent developments is experimental realization of quantum droplets, which arise in gases with strong dipole-dipole interactions [1, 2] and in two-component Bose-Einstein condensates [3, 4]. In particular, experiments of T. Pfau group demonstrated that, under appropriate tuning of the interparticle interactions, ensembles of droplets can form in strongly dipolar dysprosium gases. When these droplets overlap, they maintain global phase coherence [5], signaling the emergence of a supersolid—an exotic quantum phase whose existence has been discussed on theoretical grounds since the late fifties of the last century [6–10].

The supersolid phase uniquely combines properties of superfluidity and crystalline structure, exhibiting simultaneous off-diagonal long-range order (phase coherence) and periodic density modulations. In dipolar Bose gases, the formation of such a phase is closely linked to the presence of a roton instability in the excitation spectrum [11], which acts as a precursor to spatial ordering and droplet formation. Consequently, the coexistence of spatial structure and superfluidity has been demonstrated in arrays of quantum droplets composed of dysprosium or erbium atoms [12–20]. Other methods of forming supersolids exploit atoms resonantly coupled to an optical cavity [21, 22] or spin-orbit coupling [23]. Supersolid systems offer a promising platform for investigating the interplay between quantum coherence, collective excitations, and spontaneous symmetry breaking in low-temperature many-body physics.

In Ref. [24], we discuss the emergence of a supersolid phase in a quasi-one-dimensional mixture of a dipolar Bose-Einstein condensate and a degenerate Fermi gas. Bose-Fermi mixtures are currently the subject of intensive experimental investigation [25–27]. In [24], we observed a transition from a Bose-Einstein condensate to a supersolid phase induced by the presence of fermions. For this transition to occur, it is essential that bosonic and fermionic atoms attract each other. When this attraction becomes sufficiently strong, a roton instability

develops, leading to modulations in both bosonic and fermionic densities. This happens because, as the boson-fermion interaction strength increases, the short-range part of the effective bosonic interaction becomes attractive, while the long-range part remains repulsive. For a fixed number of fermions, the number of resulting density peaks depends primarily on the number of bosonic atoms and can range from two up to the total number of fermions. Typically, the number of fermions is much smaller than the number of bosons. For example, in the case studied in Ref. [24], the number of fermions was set to ten, while the number of bosons was on the order of several thousand.

To summarize (see Ref. [24]), the Bose-Fermi mixture enters different phases depending on the strength of the attraction between bosons and fermions. When the attraction is weak, the bosonic and fermionic clouds overlap and exhibit Friedel oscillations. With stronger attraction, a dipolar Bose-Fermi droplet forms at a critical value of the interaction strength, g_{BF} . This occurs because the interaction between all atoms becomes attractive, analogous to the formation of bright solitons or nondipolar quantum droplets in Bose-Fermi mixtures (see Refs. [28–30]). Then, the roton instability develops, and the system enters the supersolid phase. This can be confirmed by checking for the possibility of exciting the out-of-phase Goldstone mode (see movies at Ref. [31]). With even stronger attraction, the fermionic cloud breaks up, though the bosonic background remains (the self-pinning transition takes place, see also [32]). This remains the supersolid phase, but with additional phonon-like modes.

In this paper, we study the possibility of inducing a transition to the supersolid phase through a dynamic change in the boson-fermion attraction strength. Our numerical simulations resemble real experiments in which the bosonic scattering length is tuned using ramps in external magnetic fields lasting a few tens of milliseconds [12, 13].

The paper is organized as follows. In Sec. II we introduce the model of a mixture of dipolar Bose-Einstein condensate and degenerate Fermi gas. Then (Sec. III) we discuss the results of numerical simulations in which

we increase the attraction between bosons and fermions in time (i.e. perform a quench), forcing the dynamical transition to the supersolid. Sec. IV supports the possibility of the appearance of supersolid phases in systems with atoms of smaller magnetic moment. We conclude in Sec. V.

II. METHOD

We consider an atomic Bose-Fermi mixture at zero temperature and assume its many-body wave function is approximated by a product of Hartree ansatz for bosons and the Slater determinant for fermions

$$\Psi(\mathbf{x}_1, \dots, \mathbf{x}_{N_B}; \mathbf{y}_1, \dots, \mathbf{y}_{N_F}) = \psi_B(\mathbf{x}_1) \psi_B(\mathbf{x}_2) \dots \psi_B(\mathbf{x}_{N_B}) \times \frac{1}{\sqrt{N_F!}} \begin{vmatrix} \varphi_1(\mathbf{y}_1) & \dots & \varphi_1(\mathbf{y}_{N_F}) \\ \vdots & & \vdots \\ \varphi_{N_F}(\mathbf{y}_1) & \dots & \varphi_{N_F}(\mathbf{y}_{N_F}) \end{vmatrix}. \quad (1)$$

All bosons occupy the same single-particle state. The bosonic atoms possess a magnetic dipole moment, which is polarized along a direction perpendicular to the axis of the system's symmetry, as determined by the prolate shape of the trapping potential. Fermions are treated individually, with single-particle orbitals assigned to each fermionic atom. Since the fermionic sample is spin-polarized, the only short-range interactions considered are those between bosons, and between bosons and fermions. We further assume that bosons repel each other, while bosonic and fermionic atoms attract. The set of three-dimensional equations describing such a system reads:

$$i\hbar \frac{\partial \psi_B(\mathbf{r}, t)}{\partial t} = \left[-\frac{\hbar^2}{2m_B} \nabla^2 + V_B(\mathbf{r}) + g_B n_B(\mathbf{r}, t) + g_{BF} n_F(\mathbf{r}, t) + \int V_{DD}(\mathbf{r} - \mathbf{r}') n_B(\mathbf{r}', t) d^3\mathbf{r}' \right] \psi_B(\mathbf{r}, t) \quad (2)$$

for bosons and

$$i\hbar \frac{\partial \varphi_j(\mathbf{r}, t)}{\partial t} = \left[-\frac{\hbar^2}{2m_F} \nabla^2 + V_F(\mathbf{r}) + g_{BF} n_B(\mathbf{r}, t) \right] \varphi_j(\mathbf{r}, t) \quad (3)$$

for fermions (here j index runs over the whole set of fermionic atoms). Harmonic trapping potentials $V_{B(F)}(\mathbf{r}) = \frac{1}{2} m_{B(F)} \left[\omega_{B(F)\perp}^2 (x^2 + y^2) + \omega_{B(F)\parallel}^2 z^2 \right]$ are axially symmetric and elongated along z direction, coupling constants $g_B = 4\pi\hbar^2 a_B / m_B > 0$ and $g_{BF} =$

$2\pi\hbar^2 a_{BF} / \mu < 0$ are related to the scattering lengths a_B and a_{BF} , and $\mu = m_B m_F / (m_B + m_F)$ is the reduced mass of bosonic and fermionic atoms. The long-range dipolar interaction term, assuming magnetic moments are polarized along x direction, is given by

$$V_{DD}(\mathbf{r}) = \frac{\mu_{dip}^2}{r^3} \left(1 - 3 \frac{x^2}{r^2} \right), \quad (4)$$

where μ_{dip} is the magnetic moment of bosonic atom. The Eqs. (2) and (3), but without dipolar term, were used to study the formation of Bose-Fermi solitons [28, 33] whose existence has been recently confirmed experimentally [34].

We then reduce the geometry of the system to quasi-one-dimensional one. Following the standard approach, the condensate wave function $\psi_B(\mathbf{r}, t)$ and fermionic orbitals $\varphi_j(\mathbf{r}, t)$ are assumed to be in their ground states in radial directions. After integrating over radial dimensions, Eqs. (2) and (3) become

$$i\hbar \frac{\partial \psi_B(z, t)}{\partial t} = \left[-\frac{\hbar^2}{2m_B} \frac{\partial^2}{\partial z^2} + V_B(z) + g_b n_B(z, t) + g_{bf} n_F(z, t) + \int V_{dd}(z - z') n_B(z', t) dz' \right] \psi_B(z, t) \quad (5)$$

and

$$i\hbar \frac{\partial \varphi_j(z, t)}{\partial t} = \left[-\frac{\hbar^2}{2m_F} \frac{\partial^2}{\partial z^2} + V_F(z) + g_{bf} n_B(z, t) \right] \varphi_j(z, t). \quad (6)$$

All coupling constants get rescaled as $g_b = g_B / (2\pi L_\perp^2)$, $g_{bf} = g_{BF} / (2\pi L_\perp^2)$, and $\mu_d = \mu_{dip} / L_\perp$, where $L_\perp = \sqrt{\hbar / (m_B \omega_{B\perp})}$ (to simplify further analysis we assume equal radial characteristic length scales for bosons and fermions, i.e., $m_B \omega_{B\perp} = m_F \omega_{F\perp}$). As a result of reducing procedure the dipolar interaction, $V_{dd}(z)$, itself is changed. It splits into $V_{dd}(z) = V_{dd}^{sr}(z) + V_{dd}^{lr}(z)$, where the attractive short-range part equals $V_{dd}^{sr}(z) = -2/3 \mu_d^2 \delta(z)$ and the repulsive long-range part reads

$$V_{dd}^{lr}(z) = \mu_d^2 \frac{-2\sqrt{a}|z| + \sqrt{\pi} e^{\frac{z^2}{4a}} (z^2 + 2a) \operatorname{erfc}(\frac{|z|}{2\sqrt{a}})}{8a^{3/2}}, \quad (7)$$

where $a = L_\perp^2 / 2$ and erfc function is the complementary error function. The Fourier transform of $V_{dd}(z)$, which is used to solve Eq. (5) numerically, is [35]

$$\tilde{V}_{dd}(k) = \mu_d^2 f(k^2 a) + \frac{1}{3} \mu_d^2. \quad (8)$$

Here, $f(k) = k e^k \operatorname{Ei}(-k)$, where Ei is the exponential integral function.

III. QUENCH INDUCED SUPERSOLID PHASE

In contrast to Ref. [24], we investigate a dynamic method of inducing the supersolid phase in a Bose-Fermi mixture. Following experimental procedures, we vary the strength of the interactions between bosons and fermions over time. Initially, the system is prepared outside the parameter range corresponding to the supersolid phase (as discussed in [24]), within a trapping potential that is perturbed in a way that breaks the parity symmetry of the system Hamiltonian, [24]. Subsequently, the coupling parameter g_{BF} is varied dynamically to reach the supersolid regime. As expected, in the final state, we observe characteristic density modulations. Breaking the parity symmetry in the initial state is intended to trigger excitations characteristic of the supersolid phase. Indeed, these excitations can be observed, but only when the quench time is appropriately chosen. In particular, we can explicitly observe the out-of-phase and in-phase Goldstone modes, as well as the Higgs mode.

All numerical results presented below are intended to model a mixture of fermionic ^6Li and bosonic ^{162}Dy atoms. However, in Sec. IV, we present scaling arguments showing that mixtures containing less magnetic atoms, such as chromium and even rubidium, can also exhibit the supersolid phase.

The parameters are: $N_B = 3000$, $N_F = 10$, $\mu_d = 0.06$ (in units of $(\hbar\omega_{B\perp} L_\perp)^{1/2}$), and $g_B = 0.02$ (in units of $\hbar\omega_{B\perp} L_\perp^3$). The initial state of the Bose-Fermi mixture is prepared as the ground state with $g_{BF} = -1.2$ (in units of $\hbar\omega_{B\perp} L_\perp^3$), in the perturbed trapping potential. The quench to the final value of the boson-fermion attraction $g_{BF} = -3.8$ is linear in time and takes 500 (in units of $1/\omega_{B\perp}$). After quenching, the system enters the supersolid phase (see Fig. 3 in [24]), which is proved by studying the excitation spectrum. This spectrum is extracted by calculating the Fourier transform of the bosonic density $n_B(z, t)$ in both space and time and integrating out the momentum dependence

$$\widetilde{n}_B(\omega) = \int |\widetilde{n}_B(k, \omega)| dk, \quad (9)$$

where

$$\widetilde{n}_B(k, \omega) = \int \int n_B(z, t) e^{i\omega t} e^{ikz} dz dt, \quad (10)$$

all after the quench is complete.

For $g_B = 0.02$, i.e. in the range of parameters before the self-pinning transition occurs [24], the low-energy excitation spectrum is depicted in Fig. 1. There are three distinct peaks visible in the spectrum. These are the in-phase, out-of-phase Goldstone and the Higgs modes (with decreasing frequency). The out-of-phase mode is further analyzed in Fig. 2 (upper frame). The anticorrelation between the relative heights of the two density maxima (imbalance indicating the flow of the superfluid) and the position of the center of mass of two density peaks (indicating the position of the crystal-like structure) is clearly

visible. As the imbalance grows (superfluid flows to the right) the crystal-like structure moves to the left. This anticorrelation behavior, which is also supported by the movie at Ref. [31], manifests the out-of-phase character of the mode considered. Conversely, for the in-phase Goldstone mode, the superfluid and the crystal structure move together (see the lower frame in Fig. 2 and the movie at [31]).

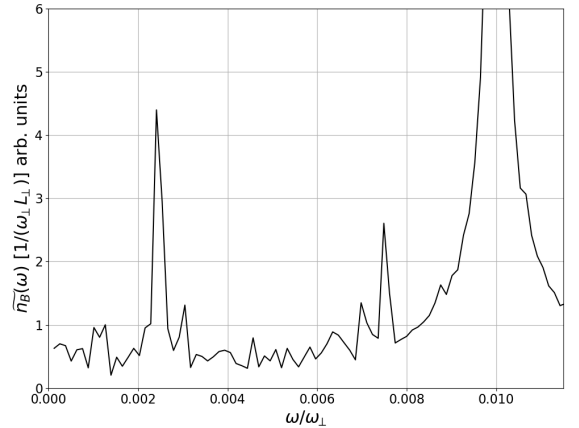


FIG. 1: Low-energy excitation spectrum of the bosonic component after a quench: $g_{BF} = -1.2 \rightarrow g_{BF} = -3.8$, at constant $g_B = 0.02$, within a duration of 500. Three peaks are clearly visible, representing the in-phase Goldstone mode at $\omega = 0.1$, the out-of-phase Goldstone mode at $\omega \approx 0.008$, and the Higgs mode at $\omega \approx 0.002$. See movies available at Ref. [31], showing the dynamics of the Goldstone and Higgs modes.

For $g_B = 0.0055$, i.e. in the range of parameters in the self-pinning region [24], the low-energy excitation spectrum is shown in Fig. 3. Similarly to Fig. 1, the distinct peaks represent the in-phase Goldstone mode at $\omega = 0.1$, the out-of-phase Goldstone mode at $\omega \approx 0.008$, and the Higgs mode at $\omega \approx 0.002$. The out-of-phase character of the out-of-phase Goldstone mode is clearly visible in Fig. 4 (upper frame) and in the movie at [31].

In both cases discussed above, the quench duration was equal to 500, as this is the value for which the out-of-phase Goldstone mode is clearly observed in the excitation spectrum. Presence of the out-of-phase Goldstone mode confirms that at the end of the quench, the system is in the supersolid phase. Interestingly, regardless of the observed density peaks for somewhat different values of the quench rate, we do not find a significant out-of-phase Goldstone mode in the excitation spectrum. This is likely due to the way the system evolves during the variation of g_{BF} over time, particularly in view of the complex excitation spectrum of the Bose-Fermi mixture, which exhibits a number of crossings and anticrossings (see [24]). A similarly rich excitation spectrum was previously reported for a dipolar dysprosium Bose-Einstein condensate, where crossings or repulsions between Bogoliubov-de Gennes modes were observed as a function of the bosonic scattering length (see [36]). Therefore,

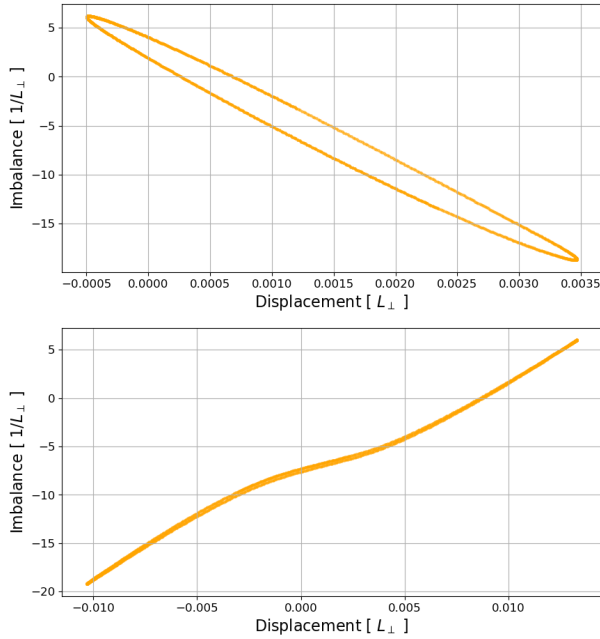


FIG. 2: Correlation between the imbalance and the displacement for out-of-phase (upper frame) and in-phase (lower frame) Goldstone modes. The modes are excited after quenching: $g_{BF} = -1.2 \rightarrow g_{BF} = -3.8$, with constant $g_B = 0.02$, within a duration of 500. The imbalance is defined as the difference in density between the right and left peaks. Displacement is defined as the average of the left and right peaks CM positions: $(z_{CM}^L + z_{CM}^R)/2$. Here, $z_{CM}^L = \int_{-\infty}^0 z n_B(z) dz$ and $z_{CM}^R = \int_0^{\infty} z n_B(z) dz$.

depending on the rate of change of the interspecies interaction, the Landau-Zener formula predicts different branching ratios for the occupation of various excited states, so the out-of-phase Goldstone mode can be only barely, if at all, excited if the duration of the quench is not properly adjusted. Our numerical protocol mimics the experimental work, Ref. [13], in which a quench of a particular duration is performed at the final stage to observe the desired feature in excitations.

IV. SUPERSOLID PHASE WITH ATOMS OF SMALLER MAGNETIC MOMENT

The numerical results presented above can be used to model a mixture of fermionic ${}^6\text{Li}$ and bosonic ${}^{162}\text{Dy}$ atoms. The magnetic dipole moment of the bosonic atoms is given by $\mu_{dip} = \tilde{\mu}_d \hbar^{5/4} (m_B^3 \omega_{B\perp})^{-1/4}$, where $\tilde{\mu}_d$ ($= 0.06$ in the calculations of Sec. III) is the dimensionless value of magnetic moment used in our numerical simulations in quasi-one-dimensional geometry. The value of the magnetic moment equal to $\tilde{\mu}_d = 0.1$ (data presented in [24]) for the trap frequency $\omega_{B\perp} = 2\pi \times 14\text{Hz}$, corresponds to $\mu_{dip} = 10\mu_B$, where μ_B is the Bohr magneton, i.e. to the magnetic moment of a dysprosium atom. At the same time, the dimensionless values of

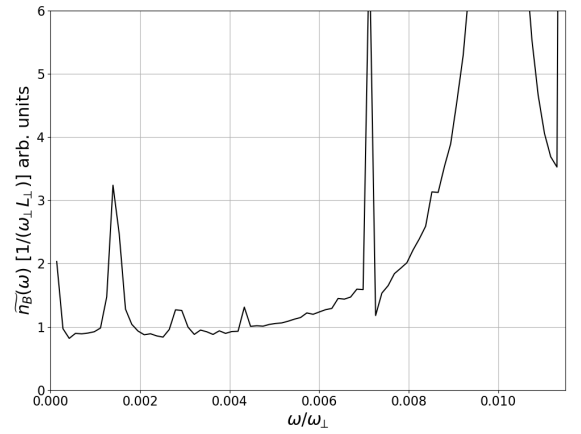


FIG. 3: Low-energy excitation spectrum of the bosonic component after a quench: $g_{BF} = -3.7 \rightarrow g_{BF} = -3.8$, at constant $g_B = 0.0055$, within a duration of 500. Three peaks are clearly visible, representing the in-phase Goldstone mode at $\omega = 0.1$, the out-of-phase Goldstone mode at $\omega \approx 0.007$, and the Higgs mode at $\omega \approx 0.001$. See movies available at Ref. [31], showing the dynamics of Goldstone modes.

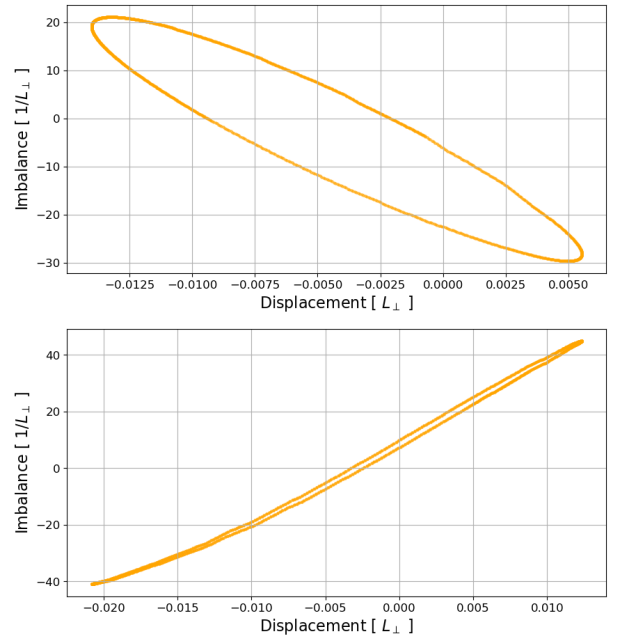


FIG. 4: Correlation between the imbalance and the displacement for out-of-phase (upper frame) and in-phase (lower frame) Goldstone modes. The modes are excited after quenching: $g_{BF} = -3.7 \rightarrow g_{BF} = -3.8$, with constant $g_B = 0.0055$, within a duration of 500.

$g_B = 0.02$ and $g_{BF} = -3.8$ translate to the scattering lengths $a_B = 3.3\text{nm}$ and $a_{BF} = -45\text{nm}$. For $\tilde{\mu}_d = 0.06$ to get the value of the magnetic moment of dysprosium atoms, one has to decrease the radial trapping frequency to $\omega_{B\perp} = 2\pi \times 1.8\text{Hz}$. This leads to larger scattering lengths of $a_B = 9.3\text{nm}$ and $a_{BF} = -127\text{nm}$.

Moreover, since $\mu_{dip} \sim \tilde{\mu}_d (m_B^3 \omega_{B\perp})^{-1/4}$, scaling our

results to those of other species is possible. For example, replacing dysprosium with chromium atoms ($m_{B,F} \rightarrow m_{B,F}/3$) and changing $\tilde{\mu}_d \rightarrow \tilde{\mu}_d/2$ and $\omega_{B\perp} \rightarrow 3^3 \omega_{B\perp}$, leads to a value of μ_{dip} that is approximately two times smaller, which is consistent with the magnetic moment of ^{52}Cr atoms. More precisely, for a radial trapping frequency of $\omega_{B\perp} = 2\pi \times 380 \text{ Hz}$ and a dipolar moment of $\tilde{\mu}_d = 0.06$, the formula $\mu_{dip} = \tilde{\mu}_d \hbar^{5/4} (m_{Cr}^3 \omega_{B\perp})^{-1/4}$ gives $\mu_{dip} = 6 \mu_B$, which is the magnetic moment of chromium atom. The scattering lengths for interactions between bosons themselves (chromium atoms) and between bosons and fermions (^2D atoms) are then $a_B = 1.1 \text{ nm}$ and $a_{BF} = -15.2 \text{ nm}$, respectively.

Further decreasing the numerical value of $\tilde{\mu}_d$, even systems consisting of non-dipolar gases such as ^{87}Rb could be considered as exhibiting supersolidity. For a radial trapping frequency of $\omega_{B\perp} = 2\pi \times 1000 \text{ Hz}$ and a value of $\tilde{\mu}_d = 0.02$ (unpublished data), the formula $\mu_{dip} = \tilde{\mu}_d \hbar^{5/4} (m_{Rb}^3 \omega_{B\perp})^{-1/4}$ gives $\mu_{dip} \approx 1 \mu_B$, which is consistent with the magnetic moment of a rubidium atom. The scattering lengths for interactions between bosons (rubidium atoms) and between bosons and fermions (^3He atoms) are then $a_B = 0.6 \text{ nm}$ and $a_{BF} = -7.6 \text{ nm}$, respectively.

In general, when planning to work with a particular atomic system, it is important to remember that the scattering lengths, which are determined by the value of the external magnetic field, are $a_B, a_{BF} \sim (m_B \omega_{B\perp})^{-1/2}$ (given the dimensionless values of the interaction strengths g_B and g_{BF}) and $\mu_{dip} \sim \tilde{\mu}_d (m_B^3 \omega_{B\perp})^{-1/4}$. In order to minimize three-body losses, the scattering lengths a_B and a_{BF} must be kept small, i.e. away from

the Feshbach resonance. It is then beneficial to have strong radial trapping and balance the atomic magnetic moment by adjusting the value of $\tilde{\mu}_d$.

V. SUMMARY

In summary, we have studied the dynamics of a mixture of dipolar condensate and degenerate Fermi gas in a quasi-one-dimensional geometry, after quenching the interaction between bosons and fermions. For appropriately chosen the final strength of the boson-fermion attraction, the system enters the supersolid phase. The appearance of the supersolid is proved by finding the out-of-phase Goldstone mode in the system excitation spectrum, both for parameters corresponding to the region before and after the self-pinning transition (see Ref. [24]). We also argue that the supersolid phase can be observed with atoms of smaller magnetic moment.

Acknowledgments

The authors were supported by the NCN Grant No. 2019/32/Z/ST2/00016 through the project MAQS under QuantERA, which has received funding from the European Union's Horizon 2020 research and innovation program under grant agreement No. 731473. Part of the results were obtained using computers of the Computer Center of University of Białystok.

-
- [1] H. Kadau, M. Schmitt, M. Wenzel, C. Wink, T. Maier, I. Ferrier-Barbut, and T. Pfau, *Nature* **530**, 194 (2016).
 - [2] L. Chomaz, S. Baier, D. Petter, M.J. Mark, F. Wächtler, L. Santos, F. Ferlaino, *Phys. Rev. X*, **6**, 041039 (2016).
 - [3] C.R. Cabrera, L. Tanzi, J. Sanz, B. Naylor, P. Thomas, P. Cheiney, and L. Tarruell, *Science* **359**, 301-304 (2017).
 - [4] G. Semeghini, G. Ferioli, L. Masi, C. Mazzinghi, L. Wolswijk, F. Minardi, M. Modugno, G. Modugno, M. Inguscio, M. Fattori, *Phys. Rev. Lett.* **120**, 235301, (2018),
 - [5] I. Ferrier-Barbut, H. Kadau, M. Schmitt, M. Wenzel, and T. Pfau, *Phys. Rev. Lett.* **116**, 215301 (2016).
 - [6] M. Boninsegni and N.V. Prokof'ev, *Rev. Mod. Phys.* **84**, 759 (2012).
 - [7] O. Penrose and L. Onsager, *Phys. Rev.* **104**, 576 (1956).
 - [8] E.P. Gross, *Phys. Rev.* **106**, 161 (1957).
 - [9] A.F. Andreev and I.M. Lifshitz, *Sov. Phys. JETP* **29**, 1107 (1969).
 - [10] A.J. Leggett, *Phys. Rev. Lett.* **25**, 1543 (1970).
 - [11] L. Santos, G.V. Shlyapnikov, and M. Lewenstein, *Phys. Rev. Lett.* **90**, 250403 (2003).
 - [12] L. Tanzi, S.M. Roccuzzo, E. Lucioni, F. Famà, A. Fioretti, C. Gabbanini, G. Modugno, A. Recati, and S. Stringari, *Nature* **574**, 382 (2019).
 - [13] M. Guo, F. Böttcher, J. Hertkorn, J.-N. Schmidt, M. Wenzel, H.P. Büchler, T. Langen, and T. Pfau, *Nature* **574**, 386 (2019).
 - [14] L. Tanzi, E. Lucioni, F. Famà, J. Catani, A. Fioretti, C. Gabbanini, R.N. Bisset, L. Santos, and G. Modugno, *Phys. Rev. Lett.* **122**, 130405 (2019).
 - [15] G. Natale, R.M.V. van Bijnen, A. Patscheider, D. Petter, M.J. Mark, L. Chomaz, and F. Ferlaino, *Phys. Rev. Lett.* **123**, 050402 (2019).
 - [16] F. Böttcher, J.-N. Schmidt, M. Wenzel, J. Hertkorn, M. Guo, T. Langen, and T. Pfau, *Phys. Rev. X* **9**, 011051 (2019).
 - [17] L. Chomaz, D. Petter, P. Ilzhöfer, G. Natale, A. Trautmann, C. Politi, G. Durastante, R.M.W. van Bijnen, A. Patscheider, M. Sohmen, M.J. Mark, and F. Ferlaino, *Phys. Rev. X* **9**, 021012 (2019).
 - [18] M.A. Norcia, C. Politi, L. Klaus, E. Poli, M. Sohmen, M.J. Mark, R.N. Bisset, L. Santos, and F. Ferlaino, *Nature* **596**, 357 (2021).
 - [19] F. Böttcher, J.-N. Schmidt, J. Hertkorn, K.S.H. Ng, S.D. Graham, M. Guo, T. Langen, and T. Pfau, *Rep. Prog. Phys.* **84**, 012403 (2021).
 - [20] L. Chomaz, I. Ferrier-Barbut, F. Ferlaino, B. Laburthe-Tolra, B.L. Lev, and T. Pfau, *Rep. Prog. Phys.* **86**, 026401 (2023).

- [21] J. Léonard, A. Morales, P. Zupancic, T. Esslinger, and T. Donner, *Nature* **543**, 87 (2017).
- [22] J. Léonard, A. Morales, P. Zupancic, T. Donner, and T. Esslinger, *Science* **358**, 1415 (2017).
- [23] J.-R. Li, J. Lee, W. Huang, S. Burchesky, B. Shteynas, F.Ç. Top, A.O. Jamison, and W. Ketterle, *Nature* **543**, 91 (2017).
- [24] M. Lewkowicz, T. Karpiuk, M. Gajda, and M. Brewczyk, *Phys. Rev. A* **111**, L011301 (2025).
- [25] K. Patel, G. Cai, H. Ando, and C. Chin, *Phys. Rev. Lett.* **131**, 083003 (2023).
- [26] E. Lippi, M. Gerken, S. Häfner, M. Repp, R. Pires, M. Rautenberg, T. Krom, E.D. Kuhnle, B. Tran, J. Ulmanis, B. Zhu, L. Chomaz, M. Weidemüller, *Few-Body Syst.* **66**, 1 (2025).
- [27] G. Cai, H. Ando, S. McCusker, and C. Chin, *arXiv:2502.06266v2*.
- [28] T. Karpiuk, M. Brewczyk, S. Ospelkaus-Schwarzer, K. Bongs, M. Gajda, and K. Rzążewski, *Phys. Rev. Lett.* **93**, 100401 (2004).
- [29] D. Rakshit, T. Karpiuk, M. Brewczyk, M. Lewenstein, and M. Gajda, *New J. Phys.* **21** 073027 (2019).
- [30] D. Rakshit, T. Karpiuk, M. Brewczyk, and M. Gajda, *SciPost Phys.* **6**, 079 (2019).
- [31] M. Lewkowicz, T. Karpiuk, M. Gajda, and M. Brewczyk (2024), https://www.youtube.com/playlist?list=PLLUYgQej5frhR6hq_4wJ4mWlfSNrhW_7b.
- [32] T. Keller, T. Fogarty, and T. Busch, *Phys. Rev. Lett.* **128**, 053401 (2022).
- [33] T. Karpiuk, M. Brewczyk, and K. Rzążewski, *Phys. Rev. A* **73**, 053602 (2006).
- [34] B.J. DeSalvo, K. Patel, G. Cai, and C. Chin, *Nature* **568**, 61 (2019).
- [35] K. Pawłowski and K. Rzążewski, *New J. Phys.* **17**, 105006 (2015).
- [36] J. Hertkorn, F. Böttcher, M. Guo, J.N. Schmidt, T. Langen, H.P. Büchler, and T. Pfau, *Phys. Rev. Lett.* **123**, 193002 (2019).